CHAPTER 10

HIGH PRESSURE STUDIES OF AS-GROWN $CuInS_2$ SINGLE CRYSTALS

Page No.

10.1.	INTRODUCTION	290
10.2.	EXPERIMENTAL	291
	10.2.1. Crystal Growth	291
	10.2.2. Calibration of Bridgman WC Opposed Anvil	291
	10.2.3. High Pressure Seebeck (S) And Resistance (R) Measurements	292
10.3.	RESULTS AND DISCUSSION	295
10.4.	CONCLUSIONS.	298
	CAPTIONS TO THE FIGURES	300
	REFERENCES	307

10.1. INTRODUCTION

Several members of the I-III-VI_2 family of semiconductors have received considerable interest [1-6] because of their potential application in solar devices. These ternary compounds crystallize in the chalcopyrite structure and are direct bandgap semiconductors. Many of these compounds can be made both n- and p-type [7] by a proper adjustment of the chalcogenide content of the crystals and by the heat treatment.

Of these many ternary compounds, $CuInS_2$ has been considered for solar cell applications due to its direct bandgap of 1.5eV, which is close to the ideal value for optimum solar energy conversion i.e. the photovoltaic effect [8].

Although a great deal of work has been carried out on the electrical [9-11] and optical properties [12,13] of $CuInS_2$ and $CuInSe_2$ at normal pressure, only a limited number of such studies have been performed at high pressure. Range et al. [14] have studied structural behaviour of $CuInS_2$ under high pressure. They found that it transforms to ZnS type structure at 5GPa and 400^oC. Optical absorption studies under pressure [15] show a linear increase of direct bandgap of p-

$CuInS_2$ with pressure upto about 9GPa. This chapter deals with the results of high pressure studies on thermoelectric power and a.C resistance of single crystals of p-and n-type $CuInS_2$.

10.2. EXPERIMENTAL

10.2.1. Crystal Growth

Single crystals of $CuInS_2$ were grown by chemical vapour transport (CVT) technique using iodine as transporting agent. The complete details of the growth procedure are given in chapter 3. In this growth run, both n-type and p-type conducting crystals grew in the ampoule. This can be due to the fact that, on account of temperature gradient, the concentration of reactants is different in different regions of the ampoule.

10.2.2. Calibration Of Bridgman WC Opposed Anvil

A tungsten carbide (WC) opposed anvil apparatus [16] with pyrophillite gasket and talc or silver chloride pressure transmitting medium can be conveniently used for high pressure studies upto 100 Kbar. Before going for experimental measurements on samples, it is essential to calibrate the anvil apparatus. Bismuth I-II and III-V transitions were used

for the pressure calibration of the apparatus. A resistivity sample assembly used for calibrating the anvil set-up by the resistance measurements of the Bismuth under pressure is shown in Fig. 10.1.

The samples of Bi for resistance measurements were contained in the pyrophillite gasket with talc as the pressure transmitting medium. A four-probe technique (Fig. 10.1.) was used to evaluate the resistance of the sample Bi.

The observed variation of the resistance of Zone-refined 99.999% pure Bismuth with pressure is shown in Fig 10.2. The pressure corresponding to the load at the minimum in the resistance curve in Bi II phase was assigned the value 26.2Kbar, which is the average of Bi I-II and Bi II-III transition pressure [17]. Similarly, the pressure corresponding to the load at the mid-point of Bi III-V transition was taken to be 76.7Kbar [18]. A smooth curve through the origin and these fixed pressure points of Bi provided calibration upto 80Kbar of the above WC opposed anvil apparatus.

10.2.3. High Pressure Seebeck (S) And Resistance (R) Measurements

The simultaneous measurements of four-probe

electrical resistance (R) and thermoelectric power (S) on the $CuInS_2$ samples were carried out to about 80 Kbar in the above calibrated anvil apparatus with 12.7mm anvil face diameter. The standard cell [19] for the measurement of resistance (R) and thermoelectric power (S) is shown in Fig. 10.3. Whereas the details of the high pressure sample assembly used in the present measurements based on the design of Singh et al. [19] are shown in Fig. 10.4 [20].

For thermoelectric power (S) measurements on $CuInS_2$, a temperature gradient was provided across the specimen by a nichrome wire heater connected to a 0-10V constant voltage DC power supply, and the potentials E_N and E_M across the pairs of the chromel and Alumel wires C_1C_2 and A_1A_2 were measured respectively with a Keithley nanovoltmeter. The chromel and Alumel wires were spot welded and carefully held parallel to one another and normal to the sample lengths with their junctions pointing readily outwards so that the sample temperature difference was maintained across the leads C_1C_2 and A_1A_2.

The thermoelectric power S of the specimen was evaluated from the measured values of E_N and E_M from the

relationship [19].

$$Q = \frac{Q_A - r Q_B}{1 - r}$$

where Q_C and Q_A are the thermoelectric powers of chromel and Alumel respectively and $r = E_{AA} / E_{CC} = E_M / E_N$.

The physical properties of Chromel and Alumel used in this evaluation of TEP are tabulated in **Table 10.1.** With these values of Q for Alumel and Chromel substituted in the expression for TEP, we get

$$Q = \frac{-18.3 - 21.6r}{(1-r)}$$

$$Q = \frac{-18.3 - 21.6r}{-(r-1)}$$

$$Q = \frac{-18.3 + 21.6r}{(r-1)}$$

Using this equation, the Seebeck Coefficient S was calculated for the samples of $CuInS_2$ from the measured values of E_N and E_M at different pressures.

Whereas the a.c resistance (R_w) at various frequencies upto 66.7 KHz was measured using microprocessor based General radio LCR bridge model 1689. At any given pressure setting, R_w was determined at different frequencies W.

10.3. RESULTS AND DISCUSSION

The results of high pressure measurements on both n- and p-type $CuInS_2$ samples are shown in Figs. 10.5 and 10.6 respectively. The analysis of electrical resistance, Hall coefficient and photoluminescence data on $Cu-III-VI_2$ compounds indicates that intrinsic defects play a major role in determining their electrical properties [21]. Since Cu does not participate significantly in covalent bonding, the covalent nature of bonding is mainly due to group III and group VI atoms. Therefore the energy of formation of Cu vacancy acceptor is considerably small and vacancy concentration can be appreciable. Lewerenz et al. [22] found that CVT grown crystals exhibit a comparatively poor photoconductivity as compared to optimized $CuInS_2$ prepared with excess In. The photoluminescence peak at about 1.4eV has a large FWHM (Full Width at half the maximum) width of 0.12 eV in CVT crystals as compared to a narrow FWHM width of 0.04eV in optimized crystals. The CVT crystal therefore possess a

large concentration of defects which lead to formation of localized states close to the valence and conduction bands. Lewerenz et al. [22] have suggested that the acceptor and donor states in CVT crystals are produced by Cu and In vacancies and Fe contaminant.

The decrease in electrical resistance of $CuInS_2$ with pressure, upto about 2GPa (Fig. 10.5 and Fig. 10.6) is due to the decrease in contact resistance which is initially high. The resistance values measured at 30Hz represent nearly the dc values of resistance. In n-type material, R (w=30Hz) decreases with pressure above 3.5GPa. This is consistent with observation of decrease in S in this pressure range, since S is inversely proportional to the density of the majority carriers in semiconductors. The p-type material however shows an increase in R (w=30Hz) above 4GPa and which is consistent with small increase in S.

It is seen that R_w decreases by 3 to 4 orders of magnitude as the frequency W is increased to 66.7KHz. This suggests that at high frequencies, hopping mechanisms of electrical conduction is dominant. Theoretical studies on semiconducting materials [23] have shown that for the Bloch electrons R_w should increase with increasing W and in case of

localised electrons which conduct by hopping process, R_w decreases with increasing W. Hence in CVT $CuInS_2$ crystals the electrical conduction at high frequencies is dominated by the hopping process. In case of p-type $CuInS_2$, R_w shows a small decrease with increasing pressure at 28.7 and 66.7 KHz, while in the n-type material a small increase in R_w is observed above 3.5 GPa. At 1 KHz also the pressure variation of R_w is qualitatively different for the n-type and p-type materials. These trends show that the pressure effects on the acceptor and donor levels are dissimilar and lead to differences in the R_w in the two cases.

The rate of variation of R_w and S in both n and p-type crystals show significant changes at 2.5 and 3.5 GPa. This can be due to shift in the acceptor levels E_a relative to the top of the valence band E_v and of donor levels E_d relative to the bottom of the conduction band E_c at these pressures. These measurements do not show occurence of a first order phase transition in the pressure range investigated. Whereas in optical absorption measurements, Gonzalez et al. [15] have shown that the direct bandgap increases at the rate dE_g/dp = 0.024 eV/GPa and a phase transition occurs at a pressure of about 10.4 GPa.

10.4. CONCLUSIONS

In conclusion it may be observed that in CVT grown $CuInS_2$ crystals there is a large concentration of intrinsic defects and the electrical transport is dominated by hopping process.

TABLE 10.1 Physical Properties Of Chromel and Alumel

Material	Absolute Q-values	Magnetic Properties	Composition
Alumel	-18.3	Magnetic	90% Ni, 10% Cr
Chromel	+21.6	Non-Magnetic	98% Ni, 2% Al

CAPTIONS TO THE FIGURES

Fig. 10.1 Sample assembly of resistivity measurements for the WC opposed anvil set up.

Fig. 10.2 Variation of the resistance of zone-refined 99.999 % pure Bismuth (Bi) with pressure.

Fig. 10.3 High pressure cell for the simultaneous measurement of thermoelectric power (S) and resistance (R) using WC opposed anvil set-up.

Fig. 10.4 Sample assembly for simultaneous measurements of thermoelectric power and resistance.

Fig. 10.5 A. C. resistance R and thermoelectric power S of n-$CuInS_2$ as a function of pressure.

Fig. 10.6 A. C. resistance R and thermoelectric power S of p-$CuInS_2$ as a function of pressure.

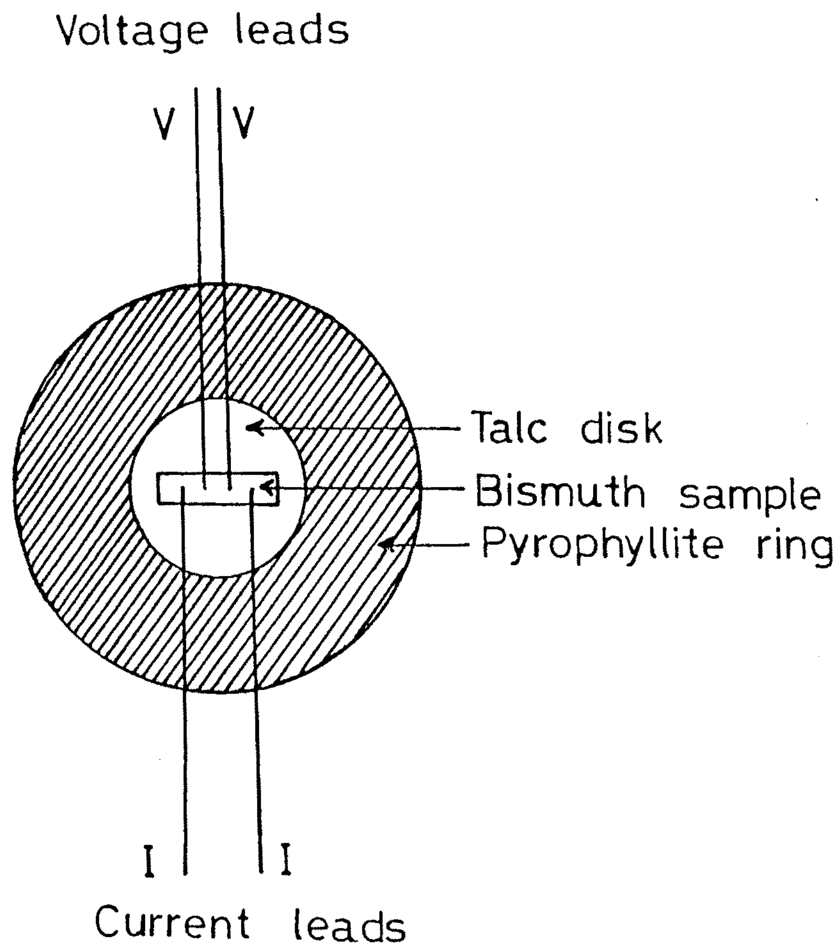

Fig 10·1

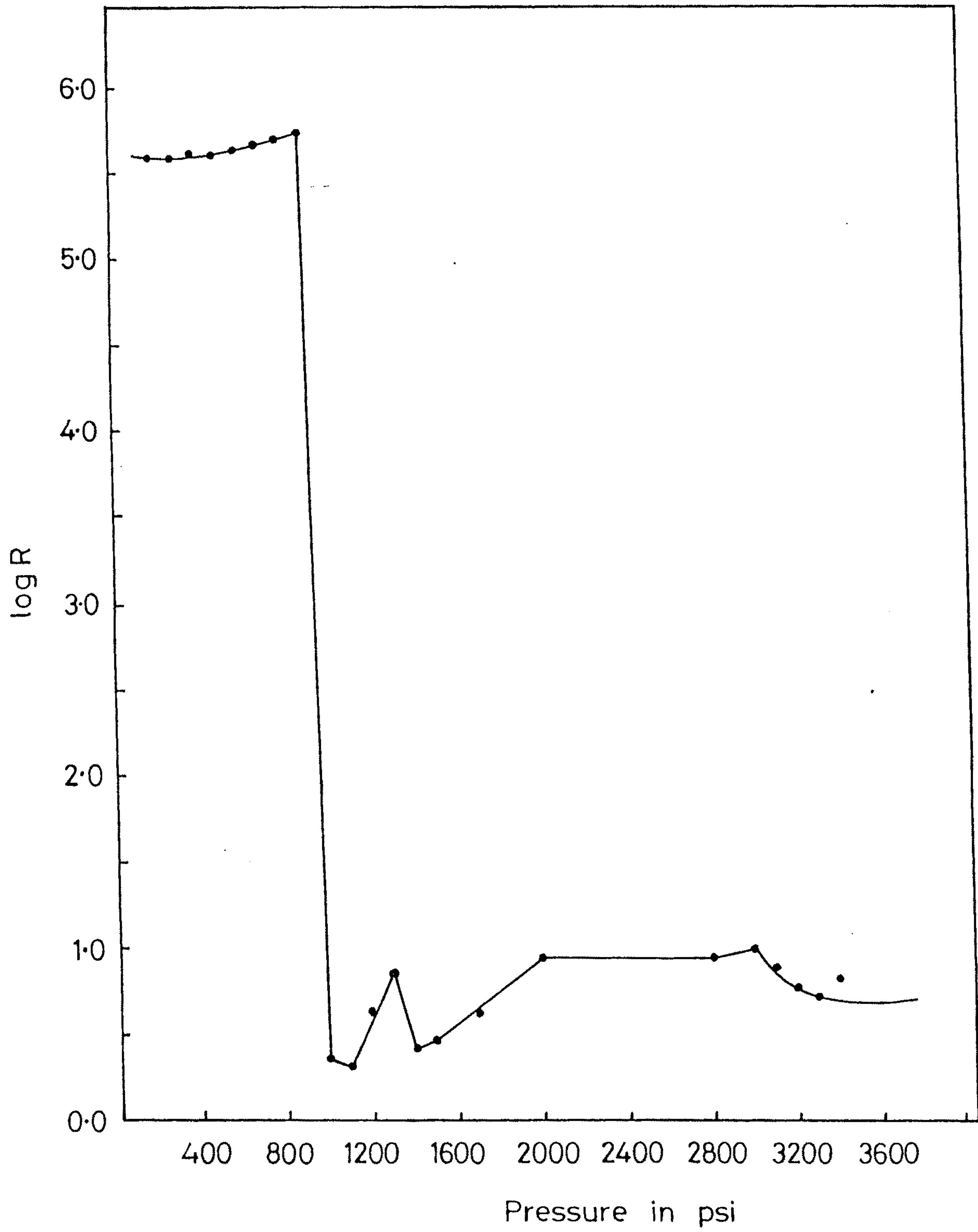

Fig 10·2

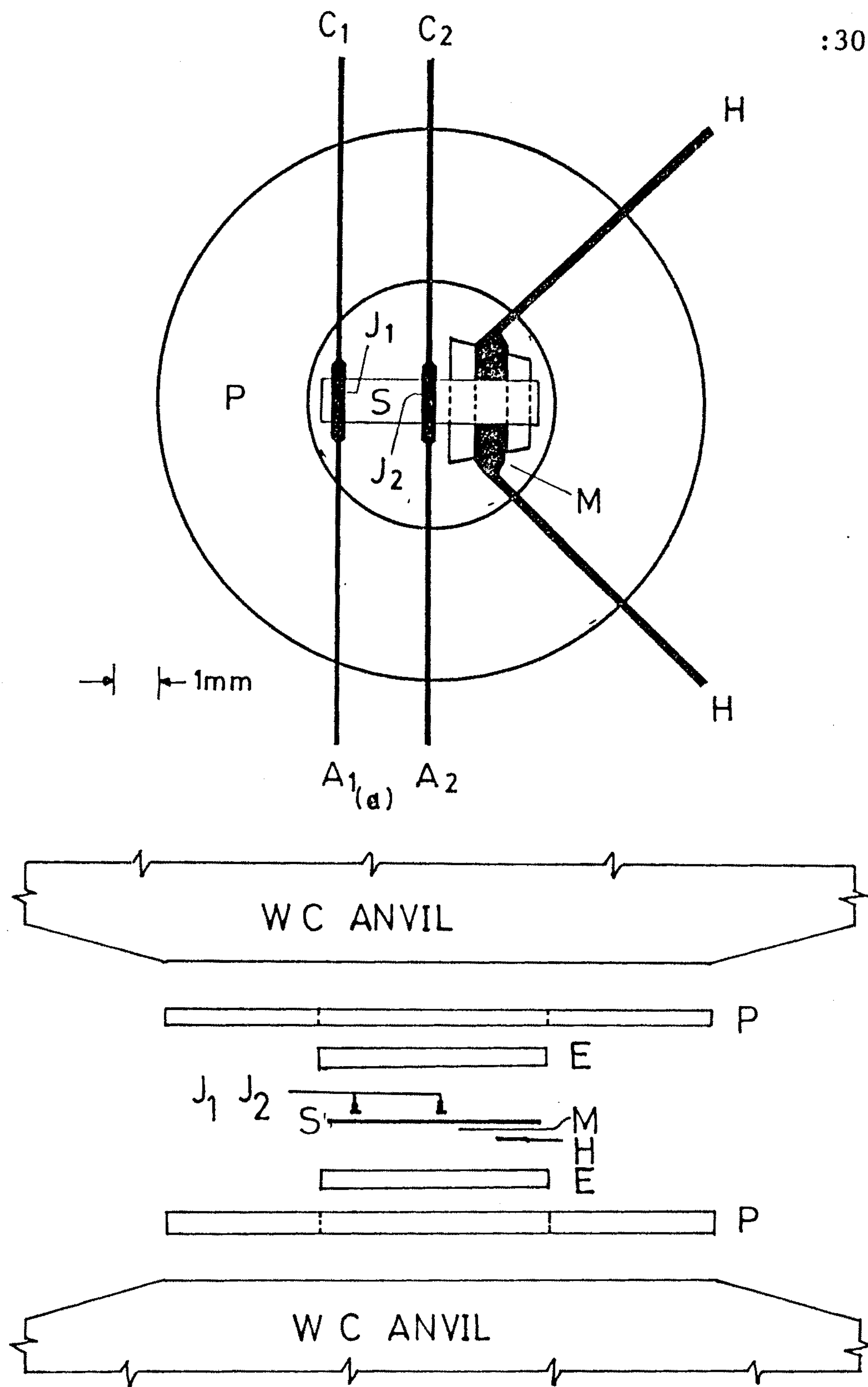

High pressure cell for the measurement of TEP using tungsten carbide opposed anvil set up [(a) View normal to the anvil face and (b) view parallel to the anvil face. P, pyrophyllite gasket E, epoxy or talc pressure transmitting disc S, specimen Heater M, mica insulation C_1 C_2 chromel A_1 A_2 alumel J_1 J_2 themrmojunctions]

fi . 10·3

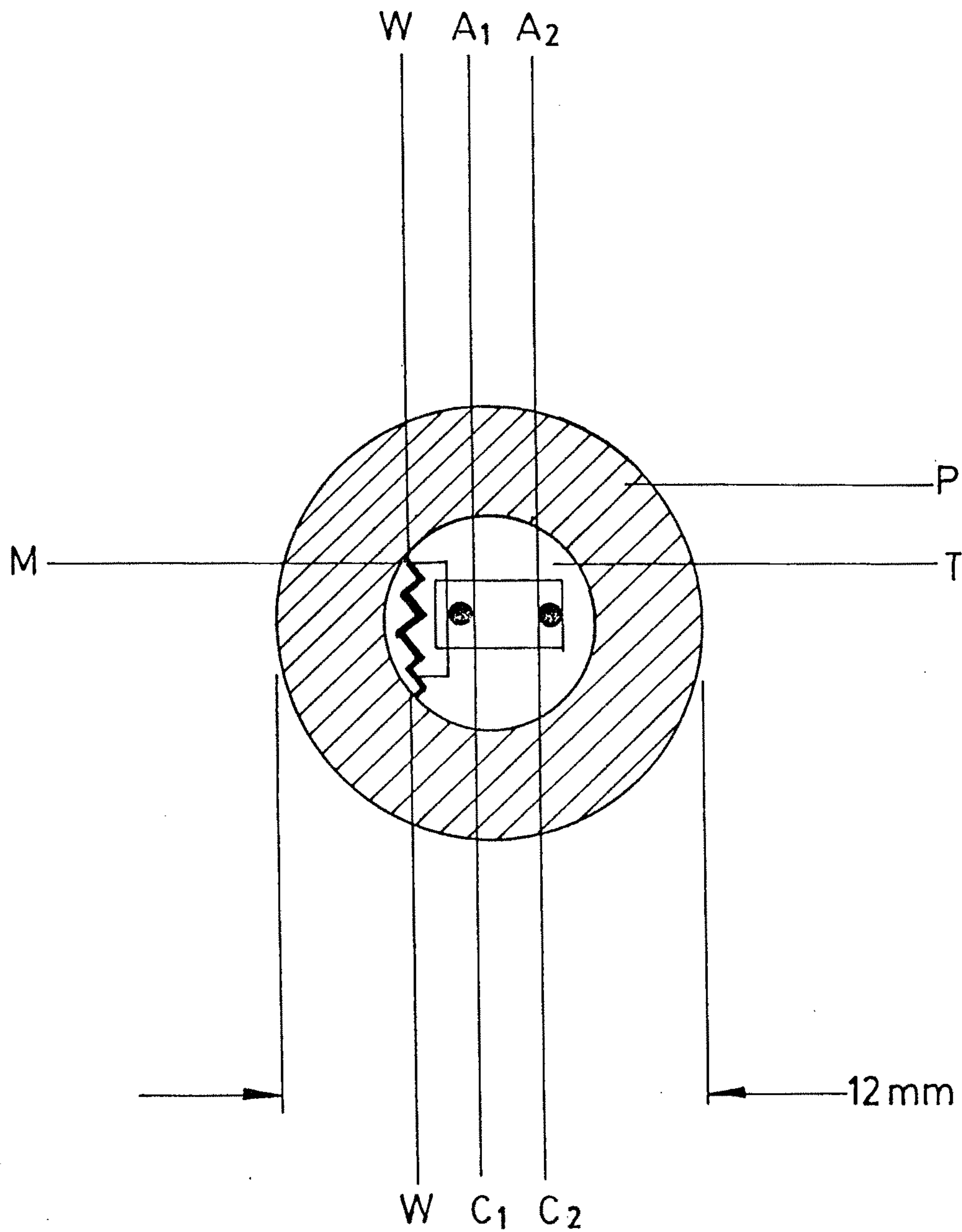

Sample assembly for Seebeck coefficient and resistivity measurements. P: pyrophyllite rings 12·50 o.d.x 5·3 mm i.d. and 0·3 mm (lower) 0·2 mm. (upper) thickness T: steatite disks; C_1 C_2, A_1 A_2: Chromel and Alumel wires 0·05 mm dia; W: Nichrome wire heater 0·03 mm dia; M: mica sheet. For the sake of clarity upper talc disk is not shown.

fig. 10·4

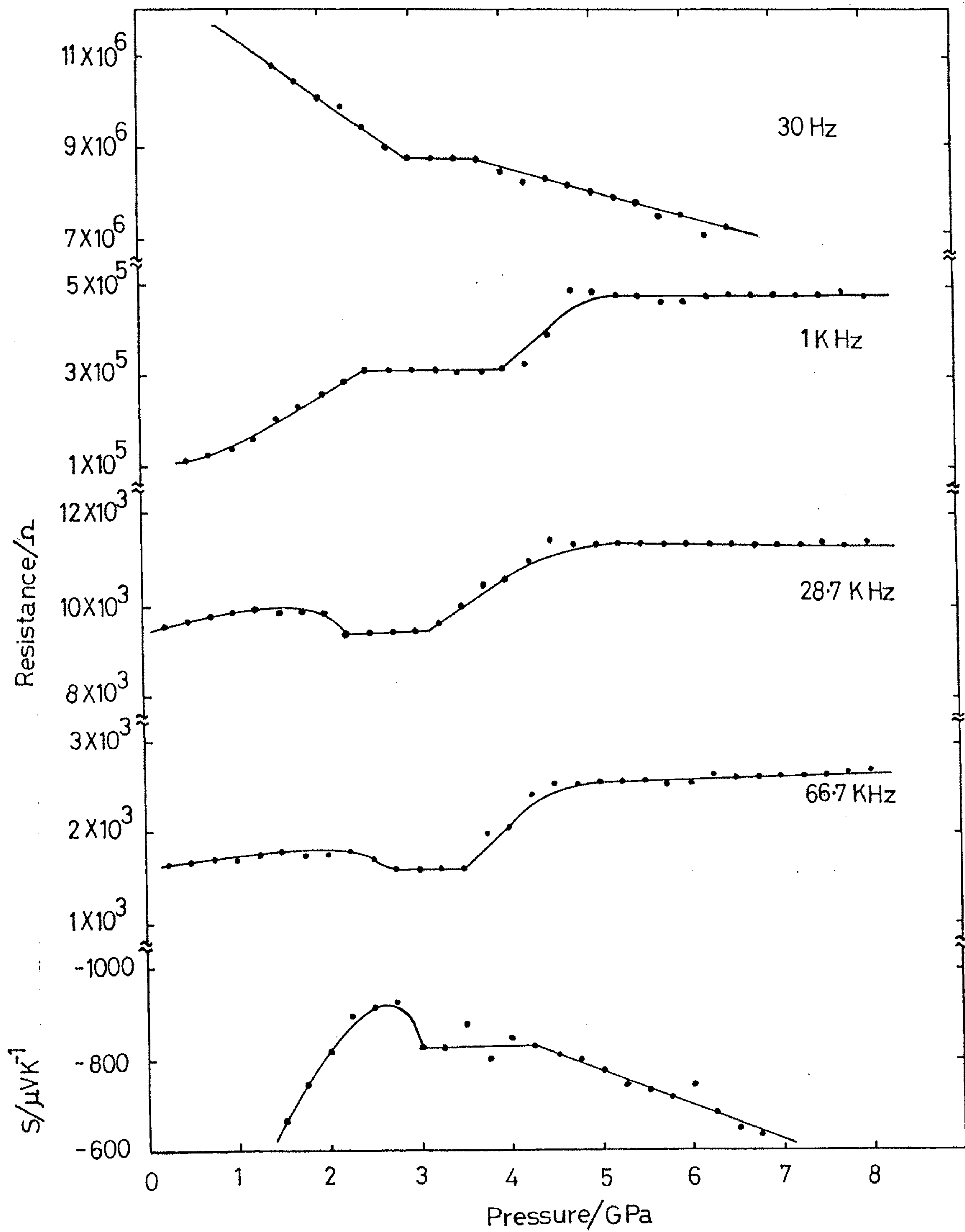

fig 10·5

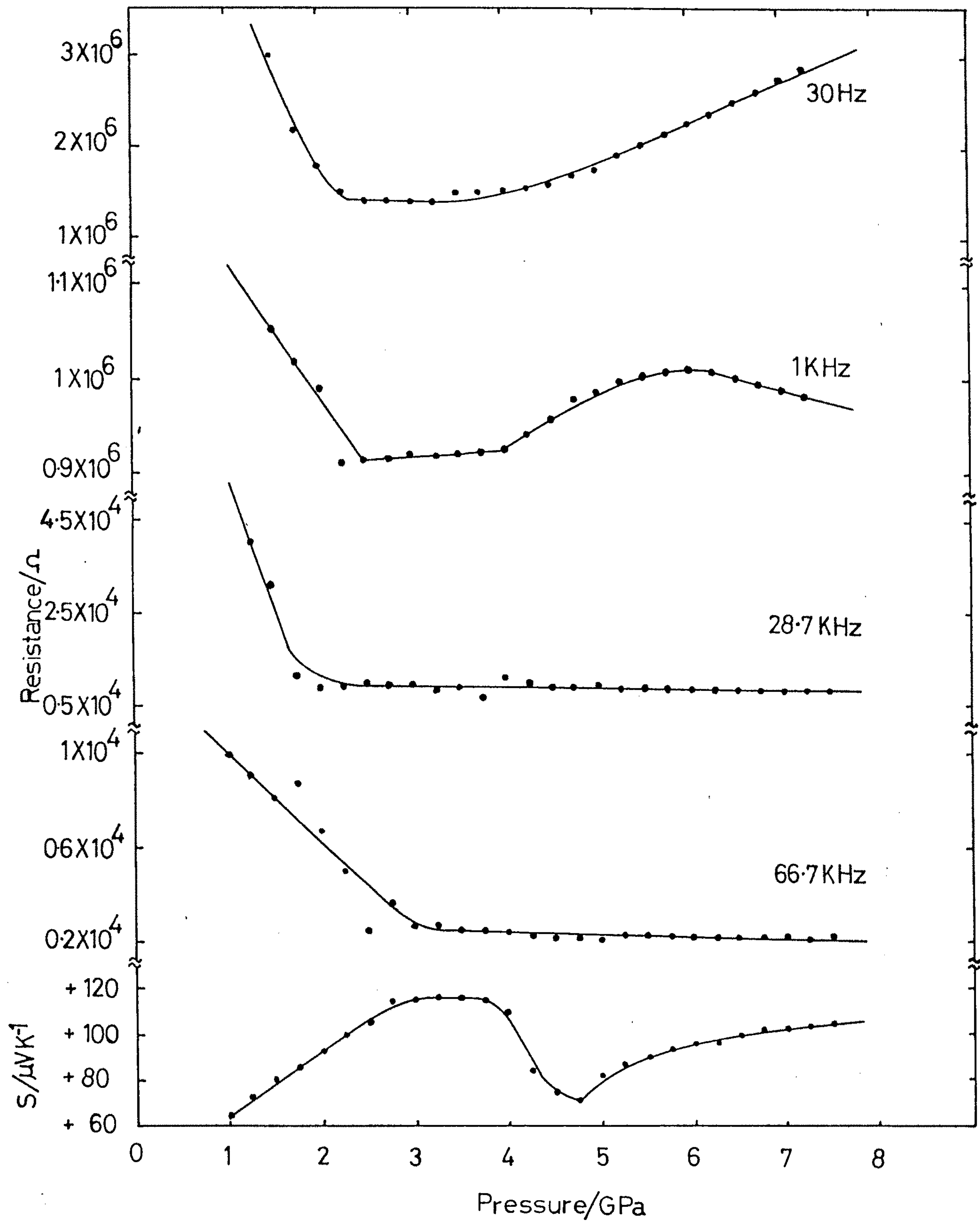

fig. 10·6

REFERENCES

1. K. W. Mitchell, G. A. Pollock and A. V. Mason; Proc. 20th IEEE Photovoltaic Specialists Conf. [Las Vegas, Nevada] p 1542 (1988).

2. H. J. Lewerenz, H. Goslowsky, K. D. Husemann and S. Fiechter; Nature **321**, 687 (1986).

3. K. W. Mitchell, C. Eberspacher, J. Ermer and D. Pier; Proc. 20th IEEE Photovoltaic specialists Conf. [Las Vegas, Nevada] (1988).

4. L. L. Kazmerski and G. A. Sanborn; J. Appl. Phys. **48**, 3178 (1977).

5. A. N. Tiwari, D. K. Pandya and K. L. Chopra; Solar Cells **22**, 263 (1987).

6. A. N. Tiwari, D. K.. Pandya and K. L. Chopra; Solar Energy Mater. **15**, 121 (1987).

7. B. Tell, J. Shay and H. Kasper; J. Appl. Phys. **43**, 2469 (1972).

8. P. M. Brindebaugh and P. Migliorata; Appl. Phys. Lett. **26**, 459 (1975).

9. S. D. Mittleman and R. Singh; Solid State Commun., **22**, 659 (1977).

10. J. L. Lin, L. M. Liu, J. T. Lue, M. H. Yang and H. L. Hwang; J. Appl. Phys. **59**, 378 (1986).

11. D. C. Look and J. C. Manthuruthil; J. Phys. Chem. Solids **37**, 173 (1976).

12. R. Tovar Barradas, C. Rincon, J. Gonzalez and G. Sanchez Perez; J. Phys. Chem. Solids **45**, 1185 (1984).

13. K. Sato, M. Isawa, N. Takahashi and M. Tsunoda; Jpn. J. Appl. Phys. **27**, 1359 (1988).

14. K. J. Range, G. Engert and Armin Weiss; Solid State Commun. **7**, 1749 (1969).

15. J. Gonzalez and C. Rincon; J. Appl. Phys. **65**, 2031 (1989).

16. V. Vijayakumar, B. K. Godwal and S. K. Sikka; Phys. Rev. **B32**, 4212 (1985).

17. G. C. Kennedy and P. N. LaMori; J. Geophys. Res. **67**, 851 (1962).

18. J. F. Cannon; J. Phys. Chem. Ref. Data **3**, 78 (1974).

19. A. K.Singh and G. Ramani; Rev. Sci. Instrum. **49**, 1324 (1978).

20. V. Vijayakumar, S. N. Vaidya, Echur V. Sampath-Kumaran and Laxmi C. Gupta; High Temp. - High Press. **12**, 649 (1980).

21. J. L.Shay and J. H. Wernick; "Ternary chalcopyrite Semiconductors : Growth, Electronic Properties and Applications" [Pergamon, New York] (1975).

22. H. J. Lewerenz, K. D. Husemann, M. Kunst, H. Goslowsky, S. Fiechter and H. Neff; J. Mater. Sci., **21**, 4419 (1986).

23. P. N. Butcher in "Handbook on Semiconductors" Vol. I Band Theory and Transport Properties, Ed. W. Paul [North-Holland Publ. Co. Amsterdam] p. 689 (1982).